Gain-of-Function Mutations of ARHGAP31, a Cdc42/Rac1 GTPase Regulator, Cause Syndromic Cutis Aplasia and Limb Anomalies

Southgate, L; Machado, RD; Snape, KM; Primeau, M; Dafou, D; Ruddy, DM; Branney, PA; Fisher, M; Lee, GJ; Simpson, MA; He, Y; Bradshaw, TY; Blaumeiser, B; Winship, WS; Reardon, W; Maher, ER; FitzPatrick, DR; Wuyts, W; Zenker, M; Lamarche-Vane, N; Trembath, RC

Gain-of-Function Mutations of *ARHGAP31*, a Cdc42/Rac1 GTPase Regulator, Cause Syndromic Cutis Aplasia and Limb Anomalies

Laura Southgate,[1,12] Rajiv D. Machado,[1,12] Katie M. Snape,[1,12] Martin Primeau,[2] Dimitra Dafou,[1] Deborah M. Ruddy,[3] Peter A. Branney,[4] Malcolm Fisher,[4] Grace J. Lee,[1] Michael A. Simpson,[1] Yi He,[2] Teisha Y. Bradshaw,[1] Bettina Blaumeiser,[5] William S. Winship,[6] Willie Reardon,[7] Eamonn R. Maher,[8,9] David R. FitzPatrick,[4] Wim Wuyts,[5] Martin Zenker,[10,11] Nathalie Lamarche-Vane[2] and Richard C. Trembath[1,3,*]

Author affiliations:

[1]King's College London, Department of Medical and Molecular Genetics, School of Medicine, Guy's Hospital, London, SE1 9RT, United Kingdom; [2]McGill University, Department of Anatomy and Cell Biology, 3640 University Street, Montreal, Quebec, Canada; [3]Department of Clinical Genetics, Guy's Hospital, London, SE1 9RT, United Kingdom; [4]MRC Human Genetics Unit, Western General Hospital, Crewe Road, Edinburgh, EH4 2XU, United Kingdom; [5]Department of Medical Genetics, University and University Hospital of Antwerp, Prins Boudewijnlaan 43, 2650 Edegem, Belgium; [6]Nelson R Mandela School of Medicine, Faculty of Health Sciences, Department of Paediatrics and Child Health, University of KwaZulu-Natal, Durban 4041, South Africa; [7]National Centre for Medical Genetics, Our Lady's Hospital for Sick Children, Crumlin, Dublin 12, Ireland; [8]Medical and Molecular Genetics, School of Clinical and Experimental Medicine, College of Medical and Dental Sciences, University of Birmingham, Institute of Biomedical Research, Birmingham, B15 2TT, United Kingdom; [9]West Midlands Regional Genetics Service, Birmingham Women's Hospital, Birmingham, B15 2TG, United Kingdom; [10]Institute of Human Genetics, University Hospital Erlangen, University of Erlangen-Nuremberg, Schwabachanlage 10, 91054, Erlangen, Germany; [11]Institute of Human Genetics, University Hospital Magdeburg, Leipziger Str. 44, 39120 Magdeburg, Germany

[12]These authors contributed equally to this work

*Correspondence: richard.trembath@kcl.ac.uk

ABSTRACT

Regulation of cell proliferation and motility is essential for normal development. The Rho family of GTPases plays a critical role in the control of cell polarity and migration through effects upon the cytoskeleton, membrane trafficking and cell adhesion. We investigated a recognized developmental disorder, Adams-Oliver syndrome (AOS), characterized by the combination of aplasia cutis congenita (ACC) and terminal transverse limb defects (TTLD). Through a genome-wide linkage analysis, we detected a locus for autosomal dominant ACC-TTLD on a region of chromosome 3q, generating a maximum LOD score of 4.93 at marker rs1464311. Candidate gene and exome-based sequencing led to the identification of independent premature truncating mutations in the terminal exon of the Rho GTPase-activating protein 31 (*ARHGAP31*) gene, which encodes a Cdc42/Rac1 regulatory protein. Mutant transcripts are stable and increase ARHGAP31 activity *in vitro* through a gain-of-function mechanism. Constitutively active ARHGAP31 mutations result in a loss of available active Cdc42 and consequently disrupt actin cytoskeletal structures. *Arhgap31* expression in the mouse is substantially restricted to the terminal limb buds and craniofacial processes during early development, closely mirroring the sites of impaired organogenesis that characterize this syndrome. These data identify the requirement for regulated Cdc42/Rac1 signaling processes during early human development.

INTRODUCTION

Members of the large family of GTPases act as molecular switches that control many aspects of cell activity, through a remarkably simple biochemical mechanism of cycling between two conformational forms. The 'active' state requires bound guanosine triphosphate (GTP) to allow interaction with one of many effector proteins, whereas the GTPase-mediated hydrolysis of GTP to guanosine diphosphate (GDP) engenders an inactive state.[1] Whilst the Rho switch appears straightforward, the process is closely controlled by at least three classes of regulators, namely guanine nucleotide exchange factors (GEFs), GTPase-activating proteins (GAPs) and GDP dissociation inhibitors (GDIs). The Rho GTPases, which include Cdc42 and Rac1, hold central functions in cell division, survival and migration, and alterations in expression have been widely studied in cancer, indicating a role in tumor invasion and metastasis.[2] However, regulation of cell proliferation and migration are also fundamental aspects of organ formation, especially during early developmental stages. We have studied an inherited disorder characterized by abnormalities of limb development, a recognized paradigm of human organogenesis, and report a GAP regulatory defect as the primary cause.

Adams-Oliver syndrome (AOS [MIM 100300]) describes the congenital absence of skin, aplasia cutis congenita (ACC), in combination with terminal transverse limb defects (TTLD) (Figure 1A). Limb abnormalities typically affect the distal phalanges or entire digits and, rarely, more proximal limb structures. Important associated anomalies include vascular cutis marmorata and cardiac and vascular abnormalities, for example pulmonary hypertension.[3] Whilst the combination of ACC and TTLD most often occurs in sporadic cases, segregation within families is consistent with autosomal dominant inheritance in some kindred and autosomal recessive in others. Variability of the disease phenotype is also widely recognized, including an absence of either of the major features in obligate

carriers, indicating reduced penetrance of the disease allele. Clinically, in cases with a known family history, the presence of either ACC or TTLD has been considered sufficient to make the diagnosis of AOS.[3]

We have now used genome-wide linkage analysis to study two kindreds with autosomal dominant ACC-TTLD and subsequently identified heterozygous mutations in a RhoGAP family member, Rho GTPase-activating protein 31 (*ARHGAP31* [MIM 610911]), also known as Cdc42 GTPase-activating protein (*CdGAP*),[4] by candidate gene and exome sequencing. We determined the distribution of expression of *Arhgap31* during development and verified the pathogenic effect of these mutations in primary human dermal fibroblasts from patients with ACC-TTLD. This genetic finding identifies the importance of Cdc42/Rac1 pathways in the developmental processes of scalp and limb formation.

SUBJECTS AND METHODS

Clinical ascertainment

Index subjects were recruited through specialist clinical genetics centers from within the UK and Europe, and via the Adams-Oliver Syndrome Support Group, UK. Additional family members, including unaffected individuals and spouses, were then invited to participate in the study. All participants underwent a detailed physical examination by experienced clinical geneticists. A diagnosis of ACC-TTLD was based on clinical guidelines[3] and supported by radiological investigations in selected patients. Kindreds AOS-5 and -12 are previously reported in the medical literature[5,6] and were updated in 2009.[3] All subjects gave written informed consent in accordance with the protocol approved by the Guy's and St Thomas' NHS Foundation Trust local research ethics

committee.

Genotyping, linkage analysis and mutation detection

Genomic DNA was extracted from peripheral venous blood by standard techniques or from saliva using the Oragene-DNA self-collection kit (DNA Genotek Inc). A genome-wide screen was performed for 22 individuals from two multigenerational families, using the GoldenGate HumanLinkage V Panel on an iScan System (Illumina Inc), following manufacturer's guidelines. Linkage analysis was performed using Merlin v1.1.2 software, under an autosomal dominant disease model with a disease allele frequency of 0.0001 and a penetrance value of 85%. Additional polymorphic markers for refinement mapping were selected with an average heterozygosity of 74%. Fluorescently-tagged polymerase chain reaction (PCR) fragments were analyzed on an ABI3730xl DNA Analyzer and genotypes were assigned using GeneMapper v3.7 software (Applied Biosystems).

All coding exons and intron-exon boundaries of the candidate genes *ARHGAP31*, *GSK3B* [MIM 605004], *LSAMP* [MIM 603241], and *POPDC2* [MIM 605823] were screened by direct DNA sequencing. Primers were designed using Primer3 software.[7] PCR products were purified with ExoSAP-IT (GE Healthcare) and sequenced using BigDye Terminator v3.1 chemistry (Applied Biosystems). Sequence traces were aligned to reference using Sequencher v4.9 software (Gene Codes Corporation).

Exome capture of subject III:2 (Figure 1B) was undertaken using the SureSelect Target Enrichment System (Agilent) and sequenced on a Genome Analyzer IIx (Illumina). Paired-end sequence reads were aligned to the reference genome (hg18) using Novoalign software (Novocraft Technologies Sdn Bhd). Duplicate reads, resulting from PCR clonality or optical duplicates, and reads mapping to multiple locations were excluded from downstream analysis. Single nucleotide substitutions and small insertion deletions

were identified and quality filtered within the SamTools software package[8] and in-house software tools.[9] Variants were annotated with respect to genes and transcripts with the SNPClassifier tool.[10] Filtering of variants for novelty was performed by comparison to dbSNP131 and 1000 Genomes pilot SNP calls (March 2010). The accession numbers of the reference sequences used for mutation nomenclature are NM_020754.2 (mRNA) and NP_065805.2 (protein).

Gene expression analysis

Fetal expression of *ARHGAP31* was assessed using a human fetal multiple tissue cDNA (MTC) panel (Clontech). PCR was performed using standard protocols with primers ARHGAP31_3Fw (5′ AGCTCATGTGACCTCACCAA 3′) and ARHGAP31_3Rv (5′ AGACTGGAGCAGGGAAGGAG 3′) to generate a 976 bp fragment. *GAPDH* primers (Clontech) were used as an internal control.

For reverse-transcription PCR (RT-PCR), cDNA was generated from 1 μg of RNA extracted from patient and wild-type (WT) EBV-transformed lymphoblasts, using the Verso cDNA kit (ABgene). Real-time quantitative PCR was performed using *ARHGAP31* Taqman gene expression probes according to the standard protocol on a Real-time PCR 7900HT (Applied Biosystems). *GAPDH* (Applied Biosystems) was used as an endogenous control. Relative levels of gene expression were calculated by SDS v2.2 software (Applied Biosystems) using the Comparative CT method of data analysis (Relative Quantity = $2^{-\Delta\Delta Ct}$).

Whole-mount *in situ* hybridization

The genomic sequence of *Arhgap31* was obtained from Ensembl. Primers were designed using Primer3 software[7] to produce a PCR product of 543 bp from the 3′ UTR of

Arhgap31 (genomic location: chr16:38,599,795-38,600,337). T3 and T7 RNA polymerase sites were added to the 5′ end of the forward and reverse primers respectively (forward: *5′ AATTAACCCTCACTAAAGG*CTGCTGGAGGAAGGTTTCTG 3′; reverse: *5′ TAATACGACTCACTATAGG*CGCCTCTCCACACCATATTT 3′). Digoxigenin (DIG) labeled (Roche Applied Science) antisense riboprobes were generated by *in vitro* transcription of purified PCR-amplified DNA template using T7 RNA polymerase.

CD1 mouse embryos at developmental stages 9.5, 10.5, 11.5 and 12.5 days post-coitum (dpc) were obtained from the Mary Lyon Centre, MRC Harwell, UK. Embryos were fixed overnight in 4% paraformaldehyde at 4 °C, stored in methanol and rehydrated in a series of graded methanol washes in PBST (PBS + 0.1% Tween 20). Proteinase K (10 μg/ml) (Roche Applied Science) permeabilization was performed for 15-35 min, depending on the stage of development. Embryos were washed twice in 0.1 M triethanolamine, with the addition of acetic anhydride to the second wash. Samples were then washed in PBST and re-fixed in 4% PFA/0.2% gluteraldehyde for 20 min. Following washing in PBST, embryos were pre-hybridized for 2 h at 60 °C and hybridized for 48 h at 60 °C in hybridization buffer containing the DIG-labeled probe. Samples were washed for 3 × 20 min in 2 × SSC + Tween 20 and then 3 × 30 min in 0.2 × SSC + 0.1% Tween 20 at 60 °C. Samples were then washed 2 × 15 min in maleic acid buffer (MAB) at room temperature. A final wash for 2 h in MAB + 2% Boehringer-Mannheim blocking reagent (BMB) + 20% heat-treated lamb serum solution at room temperature was performed before overnight incubation in the same solution containing a 1/2000 dilution of anti-DIG antibody coupled to alkaline phosphatase (Roche Applied Science). Embryos were then washed for 3 × 1 h in MAB and color detected with 2 ml of BM purple precipitating solution (Roche Applied Science).

Optical projection tomography

Whole-mount *in situ* hybridization (WISH) was performed as described above. Embryos were mounted in 1% agarose, dehydrated in methanol and then cleared overnight in BABB (1 part Benzyl Alcohol: 2 parts Benzyl Benzoate). Samples were then imaged using a Bioptonics optical projection tomography (OPT) Scanner 3001 using brightfield to detect the staining and for tissue autofluorescence (excitation 425nm, emission 475nm) to capture the anatomy.[11] The resulting images were reconstructed using Bioptonics proprietary software, automatically thresholded and merged to a single 3D image output using Bioptonics Viewer software. The downstream digital dissection and sectioning were performed using Amira software (Visage Imaging).

Cloning and mutagenesis

Full-length myc-tagged ARHGAP31 was generated as previously described.[4] Mutant constructs were engineered by performing site-directed mutagenesis with the QuickChange kit (Stratagene) on the WT template. Primers are available on request.

Cell culture

Cells were maintained at 37 °C in a humidified incubator with 5% CO_2. Human endometrioid cancer (HeLa, ATCC) and human embryonic kidney (HEK293) cells were cultured in Dulbecco's Modified Eagle's Medium (DMEM) supplemented with 4.5 g/ml GlutaMax and 10% heat inactivated fetal bovine serum (FBS). EBV-transformed lymphoblasts (ECACC) from a WT control and ACC-TTLD patients with and without *ARHGAP31* mutations were cultured in RPMI-1640 supplemented with 10% heat inactivated FBS. Human primary dermal fibroblast cells were established from 4 mm tissue biopsies from a WT control individual and an ACC-TTLD patient carrying the

p.Gln683X mutation. Tissues were enzymatically dissociated using accutase and fibroblasts were grown in basal medium 106 supplemented with 2% (v/v) FBS, 1 μg/ml hydrocortisone, 10 ng/ml human epidermal growth factor, 3 ng/ml basic fibroblast growth factor, and 10 μg/ml heparin. Normal human neonatal dermal fibroblasts (HDF, Lonza), used as an additional control for proliferation assays, were cultured under the same conditions as described above. All cell culture reagents were obtained from Invitrogen. Transient transfections of HeLa cells were performed using FuGENE (Roche) in accordance with manufacturer's instructions, using a 3:1 ratio of transfection reagent to DNA.

Immunofluorescence

HeLa cells and fibroblasts were plated in 6-well plates (Corning) on acid-treated glass coverslips (Laboratory Sales Limited) and allowed to grow until 80% confluent. Cells were fixed in ice-cold methanol, rehydrated with 1 × PBS, and blocked with a 0.5% BSA (Sigma-Aldrich) in 1 × PBS solution. Following blocking, cells were incubated with a polyclonal rabbit antibody raised against a peptide corresponding to amino acids 541-562 of mouse Arhgap31 (PRD1) and purified on a Protein A-Sepharose column (1:500 dilution). After washing with blocking solution, a secondary rabbit-specific fluorophore-tagged antibody (Abcam Inc.) was added for 1 h. Coverslips were rinsed and mounted on slides with hard-set mounting medium containing a DAPI nuclear stain (Vector Labs). Golgi and cytoskeleton visualization were performed using 58K Golgi protein and monoclonal tubulin antibodies (Abcam Inc.), respectively. Antibodies were diluted according to manufacturer's instructions. PRD1 antibody specificity tests were performed using preimmune serum from the antibody host rabbit in place of the Arhgap31 antibody. A second specificity test utilized a blocking peptide specific to the PRD1 antibody

epitope used at a 10:1 concentration (peptide to antibody). We further used a blocking peptide specific to a random region of Arhgap31 as an additional negative control. Both blocking peptides were synthesized by Sigma-Aldrich. All images were acquired on a Zeiss LSM 510 confocal microscope and processed with Adobe Photoshop. Statistical comparisons for cell rounding experiments were conducted using a Fisher's exact test.

G-LISA Cdc42 activation assay

HEK293 cells were grown to 70% confluency on 100 mm dishes and transiently transfected using polyethyleneimine (Polysciences Inc.) with 100 ng of empty vector DNA or vector encoding myc-tagged WT ARHGAP31, p.Lys1087SerfsX4 or p.Gln683X. Cells were lysed 16 h post-transfection according to manufacturer's instructions (Cytoskeleton Inc.) and snap-frozen in liquid nitrogen. Levels of tagged proteins and Cdc42 were determined by Western blotting using polyclonal myc-specific (Cell Signaling Technology) and Cdc42-specific (Santa Cruz Biotechnology) antibodies, respectively. The relative amounts of GTP-bound Cdc42 in each condition were determined in duplicate. For each Cdc42-GTP measurement, 100 µg of protein lysate was used. To compare WT and mutant ARHGAP31 activity, a student's *t*-test was used with a two-tail distribution.

Immunoprecipitation

HEK293 cells were co-transfected with mouse pRK5myc-Arhgap31 (1083-1425) and pEGFP-Arhgap31 (1-221 or 1-820). After 16 h, cells were lysed on ice in 25 mM HEPES pH 7.4, 100 mM NaCl, 10 mM $MgCl_2$, 5% glycerol, 1% NP-40, 1 mM Na_3VO_4, 10 mM NaF, 1 mM PMSF and protease cocktail inhibitors (Roche Applied Science). Protein lysates were centrifuged for 10 min at 14,000 *g* and pre-cleared for 1 h at 4 °C with

Protein G-Sepharose (GE Healthcare). Supernatants were incubated for 3 h at 4 °C with 2 μg of monoclonal myc-specific antibody (9E10) and Protein G-Sepharose. Immune complexes were washed three times in lysis buffer and resuspended in SDS sample buffer. Proteins were resolved by SDS-PAGE and detected by Western blotting using antibodies to GFP (A6455, Molecular probes) and myc.

Proliferation assay

The CyQUANT fluorescence-based microplate assay was used for quantitation of cell number. To generate a standard calibration curve, binding to cellular nucleic acids was measured using 485 nm (±10 nm) excitation and 530 nm (±12.5 nm) emission filters using a CytoFluor 2350 fluorescence microplate reader. The fluorescence emission of the dye-nucleic acid complexes was then correlated linearly with cell numbers from a dilution series ranging from 100 to 50×10^4 cells, measured using a hemocytometer.

Sample cells were lysed at room temperature with 1 ml of CyQUANT GR dye/lysis buffer and incubated in darkness for 2-5 min at room temperature. 6-well culture plates of cells were harvested on days 1-9 and lysed with 200 μl of CyQUANT GR dye/lysis buffer. Sample fluorescence was measured, and growth curves were plotted as cell number over time in culture. For each independent control (WT and HDF), an unpaired *t*-test was used to compare cultured cell numbers with the patient (p.Gln683X) sample at each time point.

Wound healing assay

Wound healing assays were performed using WT and p.Gln683X primary dermal fibroblast cells plated on fibronectin-coated 35 mm tissue culture dishes with an IBIDI chamber at a density of 8500 cells/well. Cells were serum and growth supplement starved for 12 h, before removing the cells from half of each well using a sterile rubber policeman.

Wounding was performed after 12 h incubation, cultures were washed twice with 1 × PBS and wound margins were photographed (t=0 h). The same wound margin fields were photographed at different time points, pictures were superimposed and areas were measured using Image J software.

RESULTS

Genome-wide mapping and identification of *ARHGAP31* mutations

Linkage analysis identified a locus for ACC-TTLD on chromosome 3q13.31-q13.33 (Figure S1). Subsequent refinement mapping defined a 5.53 Mb critical interval flanked by markers rs714697 and D3S4523, containing a total of 21 protein-coding genes and 3 open-reading frames (Figure S2). We sequenced four genes in affected members of the linked AOS-5 and AOS-12 families. In each kindred we identified a distinct sequence variant (c.2047C>T and c.3260delA) within the terminal coding exon of *ARHGAP31*, that segregate with the syndrome phenotype and predict the formation of premature truncating mutations (p.Gln683X and p.Lys1087SerfsX4) (Figure 1B, C). No likely disease causing sequence variants were detected in the other genes analyzed. To comprehensively exclude the existence of pathogenic mutation in the linked interval, we performed whole exome sequencing in one individual from Family AOS-12, and verified the c.2047C>T *ARHGAP31* nonsense mutation as the only novel variant within the extended 13.2 Mb linkage region (Figure S2).

We screened *ARHGAP31* by DNA sequencing in affected members of a further three multiplex kindreds, unlinked to the chromosome 3 locus, and a cohort of 43 sporadic individuals with features of ACC and TTLD, either alone or in combination. A non-synonymous polymorphism (c.2180C>T; p.Thr727Ile) was detected in two sporadic cases,

but no pathogenic sequence variants were identified in this extended cohort. To exclude the possibility that the truncating variants were also polymorphisms, or that *ARHGAP31* harbors frequent but functionally insignificant variation, we re-sequenced all 12 exons in 72 unrelated control individuals. None of these individuals carried either of the likely disease-causing *ARHGAP31* mutations or any other missense or splice-site variants. We additionally sequenced exon 12, the site of the putative disease-causing mutations, in a further 1,138 unrelated control subjects of European origin. Whilst the c.2180C>T polymorphism was detected in two control subjects, neither of the ACC-TTLD truncating mutations was detected in the combined total of over 2,000 chromosomes assayed.

ARHGAP31 expression during early development

Analysis of *ARHGAP31* transcript expression showed abundant and ubiquitous levels in all human fetal tissues examined (Figure S3). To determine the regional expression of *Arhgap31* mRNA, we studied mouse embryos during early development (Figure 2). At 9.5 dpc, the strongest expression is in the developing heart, with regional localization to the ventral walls of primitive ventricle and primitive atrium (Figures 2A and 2B). By 10.5 dpc, *Arhgap31* expression becomes largely restricted to the lateral walls of the developing ventricle, with expression in the primitive atrium becoming localized to its outer wall (Figures 2C and 2D). At 11.5 dpc, *Arhgap31* expression is largely restricted to the surface ectoderm with strong expression overlying the entire heart field, symmetrical regions of the head and flank and the apical regions of the hand and foot plates (Figures 2E and 2F). By 12.5 dpc, the expression in the surface ectoderm is not detectable by WISH (data not shown).

Effect of *ARHGAP31* mutations

To determine the impact of exon 12 mutations predicting premature termination during translation (Figure 3A), we assessed transcript stability by quantitative RT-PCR of RNA extracted from lymphoblasts. A comparison between WT control and two related subjects, both heterozygous for the c.2047C>T (p.Gln683X) mutation, showed no reduction in the abundance of *ARHGAP31* transcript, in support of the hypothesis that the mutant transcript is not removed by the process of nonsense-mediated decay (Figure 3B).

Since the antibody to ARHGAP31 was unsuitable for protein detection by Western blot analysis, we used immunofluorescence and found ARHGAP31 predominantly localized to the Golgi. We found no indication of protein degradation, such as loss of staining intensity or aggregate formation, and ARHGAP31 localization appeared normal in ACC-TTLD primary fibroblasts that harbor the p.Gln683X mutant protein (Figure 3C). However, subtle differences in localization or indeed organelle morphology, whilst not qualitatively evident, cannot be excluded.

ARHGAP31 is a member of the RhoGAP family of proteins known to inactivate the Rho GTPases Cdc42 and Rac1.[4] Thus, we next investigated the impact of truncation of ARHGAP31 on GAP activity. We performed *in vitro* experiments in HEK293 cells and found that, relative to full-length ARHGAP31, both truncated proteins displayed a marked augmentation of GAP activity upon Cdc42, resulting in a significant down-regulation of the active GTPase (Figure 4A). We conclude that both disease mutations in *ARHGAP31* behave as dominant gain-of-function alleles.

The *ARHGAP31* mutations associated with the ACC-TTLD phenotype result in the removal of the C-terminal tail. To test the possibility that the C-terminus of ARHGAP31 affects the GAP activity through intra-molecular interactions, we generated green fluorescent protein (GFP) tagged ARHGAP31 deletion constructs to perform protein

immunoprecipitation studies in HEK293 cells with a myc-tagged construct encoding the C-terminus. Indeed, we found that the C-terminus of ARHGAP31 is able to interact with the N-terminus region (amino acids 1-820), and we further refined the interaction to a region comprising the RhoGAP domain (amino acids 1-221). Although our data do not exclude the possibility that the C-terminus may also bind a second motif downstream of the RhoGAP domain, these results indicate the potential for an auto-regulation mechanism (Figure 4B).

In vitro phenotypic analysis of mutant ARHGAP31

Perturbation of Cdc42/Rac1 signaling pathways impacts directly upon cell proliferation and migration in a cell-specific manner.[12,13] Therefore, we hypothesized that the ACC-TTLD defects would impact upon cell proliferation and ordered cell migration. Following p.Gln683X fibroblasts over a 9-day period revealed a significantly reduced rate of cell proliferation (Figure 5A). In addition, we performed wound healing assays with the mutant fibroblasts, which showed significant differences in cell migration, suggestive of altered cell motility (Figures 5B and 5C). The rounding of cells is a characteristic of impairment of the ordered process of actin polymerization and associated to a specific mode of cell movement during tumor cell migration.[13] Transient transfection of disease-causing *ARHGAP31* constructs induced a rounded phenotype in a significant proportion of HeLa cells, in keeping with recent observations of suppressed Cdc42 activity (Figures 5D and 5E).[14] However, cytoskeletal organization as assessed by F-actin staining of human fibroblasts heterozygous for the p.Gln683X mutation was not qualitatively distinct from controls, presumably due to dosage compensation by the wild-type allele (data not shown).

DISCUSSION

Fundamental insight as to necessary signaling pathways requisite to normal limb patterning and outgrowth has primarily been gained from the study of model organisms and inherited disorders of limb formation.[15,16] The fibroblast growth factor (FGF), bone morphogenetic protein (BMP), hedgehog and Wnt protein families have all been implicated in this important paradigm of organogenesis. Spatial and temporal expression of these signaling molecules is critical. For example, in the apical ectodermal ridge (AER), a specialized epithelium located along the distal tip of the limb bud, molecular signals generated by several members of the *Fgf* family control limb outgrowth and proximal-distal patterning.[17] Wnt signals interact with FGFs in the AER to maintain mesenchymal progenitors in an undifferentiated, proliferative state.[18] By contrast, the expression of BMP ligands regulates dorsal-ventral patterning and interdigital cell death,[19] and inhibits sonic hedgehog transcription through disruption of FGF and Wnt signaling.[20] Further delineating the crosstalk and interaction between such genes and pathways is required to establish an integrative model of limb organogenesis; however, additional critical steps remain to be elucidated.[15]

In this study, we have used a classical positional cloning approach in conjunction with the contemporary technology of exome sequencing,[21] to identify distinct truncating mutations within the terminal exon of *ARHGAP31*. Combining candidate gene analysis with large-scale exome sequencing now provides an opportunity for rapid detection of genes in Mendelian disease. Importantly, we have shown that this strategy can be successful using exome data from a single affected individual, and have been able to verify truncating mutations of *ARHGAP31* as the only novel variation within our extended linkage interval.

The clinical phenotypes in the two kindreds with *ARHGAP31* mutations share a number

of features. Both mutations are associated with scalp aplasia cutis congenita and upper/lower limb defects of significant variability and reduced penetrance, including short distal phalanges, partial absence of the fingers and toes and cutaneous syndactyly of toes 2-3 (Figures 1B and 1C). Using whole-mount *in situ* hybridization and optical projection tomography in mouse embryos, we have detected *Arhgap31* transcript expression in distinct regions of the surface ectoderm, including the head and upper and lower limb buds, at 11.5 dpc. Expression in the distal tip of the limb buds during late stages of embryonic development would be consistent with a role in limb outgrowth and proximal-distal patterning. Interestingly, and despite evident expression of *Arhgap31* in the developing mouse heart, no affected subjects displayed evidence of congenital cardiac abnormalities, which is a widely recognized feature of the ACC-TTLD spectrum. To address this further, we screened *ARHGAP31* in an extended panel of ACC-TTLD patients, with and without cardiac abnormalities. No additional mutations were identified, indicating that defects in *ARHGAP31* account for only a small proportion of subjects with the ACC-TTLD spectrum of clinical features. Future studies will likely identify additional gene defects causative of AOS.

Our data suggest the c.2047C>T nonsense mutation does not activate the nonsense-mediated decay pathway, in keeping with premature termination codons downstream of the final splice junction.[22] Immunofluorescence studies identified the expression and localization of mutant protein to be confined to the Golgi apparatus, a site of activity of Cdc42, at comparable levels as observed for wild-type ARHGAP31.[23] The Rho family members Cdc42 and Rac1 are active when GTP bound. The hydrolysis of GTP, for example by ARHGAP31, leads to inactivation of Cdc42/Rac1 and, as such, intracellular Cdc42- and Rac1-GTP levels are inversely proportional to the activity of ARHGAP31. Measurements of GAP activity, as determined by G-LISA assays, demonstrated both

truncating mutations result in a significant down-regulation of active Cdc42, compatible with a dominant gain-of-function mechanism of these disease-causing alleles.

Both the *ARHGAP31* mutations associated with the ACC-TTLD phenotype are predicted to truncate the C-terminal tail. We postulated whether the C-terminus of ARHGAP31 was capable of interacting with the amino terminus so as to shield the RhoGAP domain, consistent with comparable auto-regulatory mechanisms reported for other members of GTPase pathways, for example p50RhoGAP, N-chimaerin, and the downstream signaling effectors WASP and PAK1.[24-27] In this study, we demonstrate an interaction between the C-terminus of ARHGAP31 and the N-terminal RhoGAP domain, suggesting a model in which truncation of the ARHGAP31 C-terminal domain in mutant proteins would result in the exposure of a constitutively active RhoGAP catalytic site (Figure 6A).

Perturbation of Cdc42 and/or Rac1 signaling impacts upon directed migration, proliferation and differentiation in a cell-specific manner.[12] Constitutive inactivation of Cdc42 by GTPase inhibitors, for example VopS, leads to cell rounding due to disruption of the actin cytoskeleton.[14] Furthermore, low Rac1 activity is associated with a rounded mode of cell movement.[28] In this report, we demonstrate a very similar outcome for cell morphology upon transient over-expression of ARHGAP31 mutant proteins, and a significant disruption of cell migration in fibroblast mutant cells, pointing towards the unregulated suppression of Cdc42/Rac1 function. Importantly, ARHGAP31 has recently emerged as a regulator of Cdc42/Rac1 signaling to the cytoskeleton, thereby playing a key role in controlling the temporal and spatial cytoskeletal remodeling necessary for the precise control of cell morphology and migration.[29] In addition, its GAP activity is regulated in an adhesion-dependent manner and appears to be required for normal cell spreading, polarized lamellipodia formation, and cell migration.[29] Whilst the wound healing assays performed in this study do not measure the direction of cell movement, it

is feasible that the increased GAP activity in ARHGAP31 mutant fibroblasts leads to a loss of adhesion and/or structural defects in cell protrusion formation, regulated by Cdc42 and Rac1,[30] thus resulting in disorganized cell migration. A more comprehensive disease cell-based study aimed, in particular, at examining cytoskeletal dysfunction is now required to build on these early observations and further define the mechanisms driving pathogenesis in this disorder.

Further insight into the wider ARHGAP31 signaling pathway is provided by a keratinocyte specific Cdc42 knock-out mouse model, which offers an integrated model for the molecular basis of the AOS phenotype.[31] Mutant mice display cellular abnormalities of skin morphogenesis, phenotypically illustrated by progressive loss of hair follicles. Central to this process is the stabilization of β-catenin by Wnt and Cdc42 signaling, which together inhibit the activity of glycogen synthase kinase 3 beta (GSK-3β), a critical driver of β-catenin degradation.[32] By contrast, ARHGAP31 levels are augmented by GSK-3β activity.[33] We would suggest that in ACC-TTLD cells, the inactivation of Cdc42 by constitutively active mutant ARHGAP31 would compromise this critical negative feedback loop and result in upregulation of mutant ARHGAP31 by GSK-3β, concomitant de-stabilization of β-catenin with consequent impairment of cellular processes, in particular progenitor cell differentiation, requisite for skin layer and hair follicle production (Figures 6B and 6C). In addition to this, Rac1 activity has recently been implicated in nuclear localization of β-catenin during canonical Wnt signaling,[34] and keratinocyte-restricted deletion has identified a critical role in hair follicle integrity.[35] More importantly, genetic removal of Rac1 in the mouse embryonic limb bud ectoderm disrupts Wnt signaling and results in severe truncations of the limb. Furthermore, conditional deletion of Rac1 in the mouse limb bud mesenchyme also leads to skeletal deformities including abnormal fusion of the skull, developmental limb defects and

syndactyly.[36] These reports, combined with our ARHGAP31 study, demonstrate the crucial roles of Cdc42 and Rac1 in skin morphogenesis and limb development. Clearly further work will now be required, informed by our genetic findings, to further elucidate these early mechanistic insights and confirm the molecular processes proposed within this model.

Taken together, our findings demonstrate that heterozygous gain-of-function mutations in *ARHGAP31* cause an autosomal dominant form of ACC-TTLD through introduction of premature termination codons in the terminal exon of the gene. Expression of *Arhgap31* during development appears confined to the limb buds, cranium and early cardiac structures, providing a remarkable correlation with the developmental defects that define ACC-TTLD. This report generates insight into the critical pathways regulating the processes of cell proliferation and movement *in vivo* and the consequences for human health with dysregulation of skin and limb formation.

SUPPLEMENTAL DATA

Supplemental Data include four figures.

ACKNOWLEDGMENTS

The authors would like to express their gratitude to the families for participating in this study. We thank all clinicians who have recruited patients to the European AOS Consortium (L. Al-Gazali, D. Amor, F. Brancati, E. Craft, B. Dallapiccola, S. Davies, C. Deshpande, J. Dixon, S. Holden, J. Hurst, P. Itin, E. Jacquemin, D. Johnson, E. Kinning, Y. Lacassie, W. Lam, A. Lampe, P. Lapunzina, M. Maniscalco, V. McConnell, L.

McGregor, V. Meiner, J. Nelson, K. Orstavik, J. Paprocka, M. Patel, S. Price, J. Prothero, E. Seemanova, M. Tekin, B. Tuysuz, A. Vandersteen and M. Whiteford.). We would also like to thank Anne Ridley for critical reading of the manuscript. This work was supported by grants from the British Heart Foundation (BHF) to R.C.T. (RG/08/006/25302), Wellcome Trust to E.R.M. and R.C.T. (078751/Z/05/Z), EU Framework 6 award for PULMOTENSION (LSHM-CT-2005-018725), Canadian Institute of Health Research grant to N.L-V. (MOP-84449) and German Research Foundation to M.Z. (ZE 524/2-2).

The authors acknowledge the use of BRC Core Facilities provided by the financial support from the Department of Health via the National Institute for Health Research (NIHR) comprehensive Biomedical Research Centre award to Guy's and St Thomas' NHS Foundation Trust in partnership with King's College London and King's College Hospital NHS Foundation Trust. R.C.T. is a senior investigator at the NIHR. R.D.M. is a BHF Intermediate Research Fellow (FS/07/036). P.B. and M.F. are Medical Research Council (MRC) career development fellows funded by the NIDCR (NIH) Craniofacial Center Grant (P50 DE-16215-05). D.R.F. is a MRC senior clinician scientist. N.L-V. is a Fonds de la Recherche en Santé du Quebec (FRSQ) chercheur-boursier senior.

WEB RESOURCES

The URLs for data presented herein are as follows:

Online Mendelian Inheritance in Man (OMIM), http://www.omim.org

Novoalign, http://www.novocraft.com

Image J software, http://rsbweb.nih.gov/ij

REFERENCES

1. Tcherkezian, J., and Lamarche-Vane, N. (2007). Current knowledge of the large RhoGAP family of proteins. Biol. Cell 99, 67-86.

2. Vega, F.M., and Ridley, A.J. (2008). Rho GTPases in cancer cell biology. FEBS Lett. 582, 2093-2101.

3. Snape, K.M., Ruddy, D., Zenker, M., Wuyts, W., Whiteford, M., Johnson, D., Lam, W., and Trembath, R.C. (2009). The spectra of clinical phenotypes in aplasia cutis congenita and terminal transverse limb defects. Am. J. Med. Genet. 149A, 1860-1881.

4. Tcherkezian, J., Triki, I., Stenne, R., Danek, E.I., and Lamarche-Vane, N. (2006). The human orthologue of CdGAP is a phosphoprotein and a GTPase-activating protein for Cdc42 and Rac1 but not RhoA. Biol. Cell 98, 445-456.

5. Verdyck, P., Blaumeiser, B., Holder-Espinasse, M., Van Hul, W., and Wuyts, W. (2006). Adams-Oliver syndrome: clinical description of a four-generation family and exclusion of five candidate genes. Clin. Genet. 69, 86-92.

6. Bonafede, R.P., and Beighton, P. (1979). Autosomal dominant inheritance of scalp defects with ectrodactyly. Am. J. Med. Genet. 3, 35-41.

7. Rozen, S., and Skaletsky, H.J. (2000). Primer3 on the WWW for general users and for biologist programmers. In Bioinformatics Methods and Protocols: Methods in Molecular Biology, S. Krawetz and S. Misener, eds. (Totowa, NJ, Humana Press), pp. 365-386.

8. Li, H., Handsaker, B., Wysoker, A., Fennell, T., Ruan, J., Homer, N., Marth, G., Abecasis, G., and Durbin, R. (2009). The Sequence Alignment/Map format and SAMtools. Bioinformatics 25, 2078-2079.

9. Simpson, M.A., Irving, M.D., Asilmaz, E., Gray, M.J., Dafou, D., Elmslie, F.V., Mansour, S., Holder, S.E., Brain, C.E., Burton, B.K., et al. (2011). Mutations in NOTCH2 cause Hajdu-Cheney syndrome, a disorder of severe and progressive bone loss. Nat. Genet. 43, 303-305.

10. Li, K., and Stockwell, T.B. (2010). VariantClassifier: A hierarchical variant classifier for annotated genomes. BMC Res. Notes 3, 191.

11. Sharpe, J., Ahlgren, U., Perry, P., Hill, B., Ross, A., Hecksher-Sorensen, J., Baldock, R., and Davidson, D. (2002). Optical projection tomography as a tool for 3D microscopy and gene expression studies. Science 296, 541-545.

12. Etienne-Manneville, S., and Hall, A. (2002). Rho GTPases in cell biology. Nature 420, 629-635.

13. Sanz-Moreno, V., and Marshall, C.J. (2010). The plasticity of cytoskeletal dynamics underlying neoplastic cell migration. Curr. Opin. Cell Biol. 22, 690-696.

14. Yarbrough, M.L., Li, Y., Kinch, L.N., Grishin, N.V., Ball, H.L., and Orth, K. (2009). AMPylation of Rho GTPases by Vibrio VopS disrupts effector binding and downstream signaling. Science 323, 269-272.

15. Zeller, R., Lopez-Rios, J., and Zuniga, A. (2009). Vertebrate limb bud development: moving towards integrative analysis of organogenesis. Nat. Rev. Genet. 10, 845-858.

16. Stricker, S., and Mundlos, S. (2011). Mechanisms of digit formation: Human malformation syndromes tell the story. Dev. Dyn.

17. Mariani, F.V., Ahn, C.P., and Martin, G.R. (2008). Genetic evidence that FGFs have an instructive role in limb proximal-distal patterning. Nature 453, 401-405.

18. ten Berge, D., Brugmann, S.A., Helms, J.A., and Nusse, R. (2008). Wnt and FGF signals interact to coordinate growth with cell fate specification during limb development. Development 135, 3247-3257.

19. Maatouk, D.M., Choi, K.S., Bouldin, C.M., and Harfe, B.D. (2009). In the limb AER Bmp2 and Bmp4 are required for dorsal-ventral patterning and interdigital cell death but not limb outgrowth. Dev. Biol. 327, 516-523.

20. Bastida, M.F., Sheth, R., and Ros, M.A. (2009). A BMP-Shh negative-feedback loop restricts Shh expression during limb development. Development 136, 3779-3789.

21. Ng, S.B., Turner, E.H., Robertson, P.D., Flygare, S.D., Bigham, A.W., Lee, C., Shaffer, T., Wong, M., Bhattacharjee, A., Eichler, E.E., et al. (2009). Targeted capture and massively parallel sequencing of 12 human exomes. Nature 461, 272-276.

22. Hentze, M.W., and Kulozik, A.E. (1999). A perfect message: RNA surveillance and nonsense-mediated decay. Cell 96, 307-310.

23. Michaelson, D., Silletti, J., Murphy, G., D'Eustachio, P., Rush, M., and Philips, M.R. (2001). Differential localization of Rho GTPases in live cells: regulation by hypervariable regions and RhoGDI binding. J. Cell. Biol. 152, 111-126.

24. Moskwa, P., Paclet, M.H., Dagher, M.C., and Ligeti, E. (2005). Autoinhibition of p50 Rho GTPase-activating protein (GAP) is released by prenylated small GTPases. J. Biol. Chem. 280, 6716-6720.

25. Colon-Gonzalez, F., Leskow, F.C., and Kazanietz, M.G. (2008). Identification of an autoinhibitory mechanism that restricts C1 domain-mediated activation of the Rac-GAP alpha2-chimaerin. J. Biol. Chem. 283, 35247-35257.

26. Lei, M., Lu, W., Meng, W., Parrini, M.C., Eck, M.J., Mayer, B.J., and Harrison, S.C. (2000). Structure of PAK1 in an autoinhibited conformation reveals a multistage activation switch. Cell 102, 387-397.

27. Devriendt, K., Kim, A.S., Mathijs, G., Frints, S.G., Schwartz, M., Van Den Oord, J.J., Verhoef, G.E., Boogaerts, M.A., Fryns, J.P., You, D., et al. (2001). Constitutively activating mutation in WASP causes X-linked severe congenital neutropenia. Nat. Genet. 27, 313-317.

28. Sanz-Moreno, V., Gadea, G., Ahn, J., Paterson, H., Marra, P., Pinner, S., Sahai, E., and Marshall, C.J. (2008). Rac activation and inactivation control plasticity of tumor cell movement. Cell 135, 510-523.

29. LaLonde, D.P., Grubinger, M., Lamarche-Vane, N., and Turner, C.E. (2006). CdGAP associates with actopaxin to regulate integrin-dependent changes in cell morphology and motility. Curr. Biol. 16, 1375-1385.

30. Hall, A. (1998). Rho GTPases and the actin cytoskeleton. Science 279, 509-514.

31. Wu, X., Quondamatteo, F., Lefever, T., Czuchra, A., Meyer, H., Chrostek, A., Paus, R., Langbein, L., and Brakebusch, C. (2006). Cdc42 controls progenitor cell differentiation and beta-catenin turnover in skin. Genes Dev. 20, 571-585.

32. Willert, K., Shibamoto, S., and Nusse, R. (1999). Wnt-induced dephosphorylation of axin releases beta-catenin from the axin complex. Genes Dev. 13, 1768-1773.

33. Danek, E.I., Tcherkezian, J., Triki, I., Meriane, M., and Lamarche-Vane, N. (2007). Glycogen synthase kinase-3 phosphorylates CdGAP at a consensus ERK 1 regulatory site. J. Biol. Chem. 282, 3624-3631.

34. Wu, X., Tu, X., Joeng, K.S., Hilton, M.J., Williams, D.A., and Long, F. (2008). Rac1 activation controls nuclear localization of beta-catenin during canonical Wnt signaling. Cell 133, 340-353.

35. Chrostek, A., Wu, X., Quondamatteo, F., Hu, R., Sanecka, A., Niemann, C., Langbein, L., Haase, I., and Brakebusch, C. (2006). Rac1 is crucial for hair follicle integrity but is not essential for maintenance of the epidermis. Mol. Cell. Biol. 26, 6957-6970.

36. Suzuki, D., Yamada, A., Amano, T., Yasuhara, R., Kimura, A., Sakahara, M., Tsumaki, N., Takeda, S., Tamura, M., Nakamura, M., et al. (2009). Essential mesenchymal role of small GTPase Rac1 in interdigital programmed cell death during limb development. Dev. Biol. 335, 396-406.

FIGURE TITLES AND LEGENDS

Figure 1. Features of ACC-TTLD and segregation of *ARHGAP31* mutations

(A) Characteristic phenotype of ACC-TTLD, with severe ACC (left panels), and a range of TTLD defects of the hands (middle panels) and feet (right panels), including partial absence of the fingers and toes, and short distal phalanxes of fingers and toes.

(B) Pedigree structure of Family AOS-12 showing segregation of the c.2047C>T nonsense mutation represented in the adjacent sequence chromatogram.

(C) Segregation and sequence chromatogram of the c.3260delA frameshift mutation in Family AOS-5. Mutation carriers are denoted by + / –.

Key to symbols: ◧ Aplasia cutis congenita; ◨ Bony defect / abnormal fontanelle; ◩ Terminal transverse limb defects; ◪ Syndactyly; ⊙ Unsymptomatic mutation carrier; □ Unaffected.

Figure 2. Expression of *Arhgap31* during mouse embryogenesis

(A) Right lateral view of volume rendered OPT 3-dimensional representation of a 9.5 dpc

mouse embryo showing *Arhgap31* expression (red) in developing heart (he).

(B) Digital section of same embryo as A, showing expression in ventral wall of the early ventricle and atrium of the heart and the first pharyngeal arch (pa).

(C) Frontal view of rendered, and (D) digital coronal section of 10.5 dpc mouse embryo with expression in the lateral walls of the early ventricles of the heart and the first pharyngeal arch derived facial mesenchyme (fm).

(E and F) By 11.5 dpc the expression is restricted to distinct regions of the surface ectoderm (se), including the upper and lower limb bud (lbe).

Figure 3. Transcript and protein expression in WT and mutant cells

(A) Schematic of the *ARHGAP31* structure, showing the position of the mutations identified in exon 12. The ARHGAP31 structure beneath depicts the known RhoGAP and proline-rich domains, a site of phosphorylation by GSK-3.

(B) Real-time quantitative RT-PCR examining *ARHGAP31* transcript levels in lymphoblasts from two related subjects heterozygous for the c.2047C>T (p.Gln683X) nonsense mutation, compared to a genotypically normal control (WT). Patient and control samples show no appreciable difference in transcript expression. Sample identifiers refer to the pedigree structure in Figure 1B. The ACC-TTLD control is a patient with no *ARHGAP31* mutation (molecular genetic basis unknown). Data represent mean ± SD from 3 independent experiments. RQ = Relative quantification.

(C) Immunostaining of (i) endogenous ARHGAP31 (red) and (ii) Golgi (green), with marked levels of co-localization to the Golgi apparatus in HeLa cells (iii). The nucleus is stained in blue. Images in the inset boxes show a 3× higher magnification of the single cell marked by the dashed lines. (iv) The high specificity of the ARHGAP31 antibody is indicated by the absence of staining in the presence of blocking peptide to the binding

epitope. In both (v) WT and (vi) mutant (p.Gln683X) fibroblasts, ARHGAP31 (green) localizes to the Golgi (red) and appears identical and of equivalent intensity. Inset boxes show 3× higher magnifications of the single cells marked.

Figure 4. Analysis of GAP activity in ARHGAP31 truncations

(A) G-LISA assays measuring the relative amounts of Cdc42-GTP levels in HEK293 cells expressing myc-tagged wild-type ARHGAP31 (full-length), p.Lys1087SerfsX4 or p.Gln683X. Relative Cdc42-GTP values are expressed as a ratio of Cdc42-GTP levels found in full-length ARHGAP31. Data are presented as mean ± SEM from 4 independent experiments. E.V. = empty vector; **P<0.0002, ***P<0.00001.

(B) Immunoprecipitation of mouse ARHGAP31 deletion constructs, to map the intramolecular interaction between C-terminal amino acids 1083-1425 and the proximal 221 residues harboring the RhoGAP domain. Full-length protein products are marked by the arrows (smaller bands represent degradation products; *IgG light chain). Levels of transfected proteins, assessed by Western blotting of the lysates with anti-myc antibody, are displayed in the lower panel.

Figure 5. Functional characterization of *ARHGAP31* mutations

(A) Bar chart comparing the proliferative activity of p.Gln683X primary dermal fibroblasts (light grey bars) with two distinct control fibroblast cell lines (black and dark grey bars). Data represent mean ± SEM for three independent experiments. Statistical analysis of each time-point (days 1-9) revealed a significant decrease in the proliferative ability of cells carrying the p.Gln683X mutation when compared independently to each of the two unaffected controls (*P<0.01). WT = primary dermal fibroblasts from a tissue biopsy; HDF = human dermal neonatal fibroblasts.

(B) Wound-healing migration assay showing coverage of a cell-free gap by primary dermal fibroblasts heterozygous for the p.Gln683X mutation and WT control fibroblasts at 24 hours post-wounding.

(C) Plot showing percentage of wound restoration at 18, 24 and 30 hours post-wounding. Fibroblasts heterozygous for the p.Gln683X mutation (light grey bars) migrate at a significantly faster rate compared to similar WT control fibroblasts (black bars). Data show means ± SEM from three independent experiments.

(D) HeLa cells transiently transfected with myc-tagged WT ARHGAP31, p.Gln683X and p.Lys1087SerfsX4 constructs. Cell shape was visualized by confocal microscopy for tubulin (red) and transfected cells identified by co-staining with fluorescent conjugated anti-myc antibody (green). DAPI was used to stain the cell nuclei (blue). Rounded cells are indicated by the white arrows and 2× higher magnifications of individual cells are shown above.

(E) Bar-chart showing the mean percentage of rounded HeLa cells observed for each ARHGAP31 construct from three independent transfection experiments (error bars denote SD).

Figure 6. Schematic of disrupted ARHGAP31 signaling

(A) Schematic representing the putative mechanism of disease. The C-terminus of ARHGAP31 inhibits the activity of the RhoGAP domain by specific interaction with amino acids 1-221 (red cross symbol). Truncated mutant proteins lacking the C-terminus would therefore be incapable of auto-inhibition, resulting in a constitutively active RhoGAP domain.

(B) Schematic of the normal ARHGAP31 signaling system. ARHGAP31 cycles Cdc42 from an active to an inactive form by hydrolysis of GTP to GDP. GSK-3β upregulates

ARHGAP31 levels, likely through phosphorylation at a consensus ERK1 site. Activated Cdc42 promotes actin polymerization and cellular processes including migration, and acts to inhibit GSK-3β activity by stimulating PKCζ phosphorylation of GSK-3β. Wnt signaling is an additional negative regulator of GSK-3β activity. Down-regulation of GSK-3β leads to decreased proteasomal degradation of cytosolic β-catenin. Active β-catenin translocates to the nucleus, whereupon the engagement of transcriptional co-factors controls the differentiation of progenitor cells in the skin.

(C) In ACC-TTLD mutant cells, constitutive activation of ARHGAP31 leads to an imbalance between active and inactive Cdc42. A decrease in the levels of active GTP-bound Cdc42 results in reduced activation of PKCζ with a concomitant increase in β-catenin degradation and disruption of cellular processes.

Key: PKCζ = Protein kinase C; GSK-3β = Glycogen synthase kinase 3 beta; P_i = Inorganic phosphate.

Figure 1

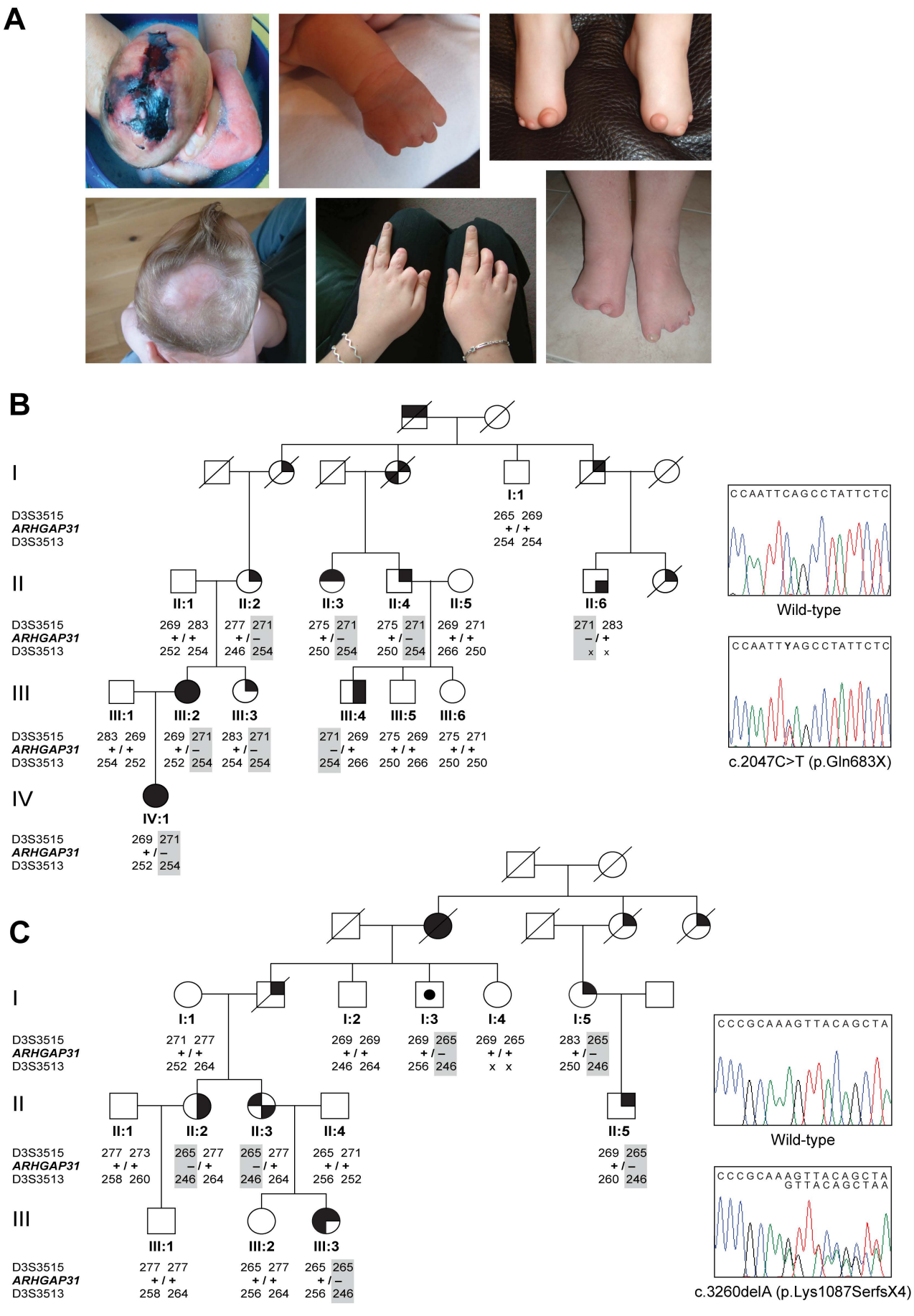
A
B
I
II
III
IV
D3S3515
ARHGAP31
D3S3513
I:1
265 269
+ / +
254 254
II:1
269 283
+ / +
252 254
II:2
277 271
+ / –
246 254
II:3
275 271
+ / –
250 254
II:4
275 271
+ / –
250 254
II:5
269 271
+ / +
266 250
II:6
271 283
– / +
x x
III:1
283 269
+ / +
254 252
III:2
269 271
+ / –
252 254
III:3
283 271
+ / –
254 254
III:4
271 269
– / +
254 266
III:5
275 269
+ / +
250 266
III:6
275 271
+ / +
250 250
IV:1
269 271
+ / –
252 254
CCAATTCAGCCTATTCTC
Wild-type
CCAATTYAGCCTATTCTC
c.2047C>T (p.Gln683X)
C
I:1
271 277
+ / +
252 264
I:2
269 269
+ / +
246 264
I:3
269 265
+ / –
256 246
I:4
269 265
+ / +
x x
I:5
283 265
+ / –
250 246
II:1
277 273
+ / +
258 260
II:2
265 277
– / +
246 264
II:3
265 277
– / +
246 264
II:4
265 271
+ / +
256 252
II:5
269 265
+ / –
260 246
III:1
277 277
+ / +
258 264
III:2
265 277
+ / +
256 264
III:3
265 265
+ / –
256 246
CCCGCAAAGTTACAGCTA
Wild-type
CCCGCAAAGTTACAGCTA
GTTACAGCTAA
c.3260delA (p.Lys1087SerfsX4)

Figure 2

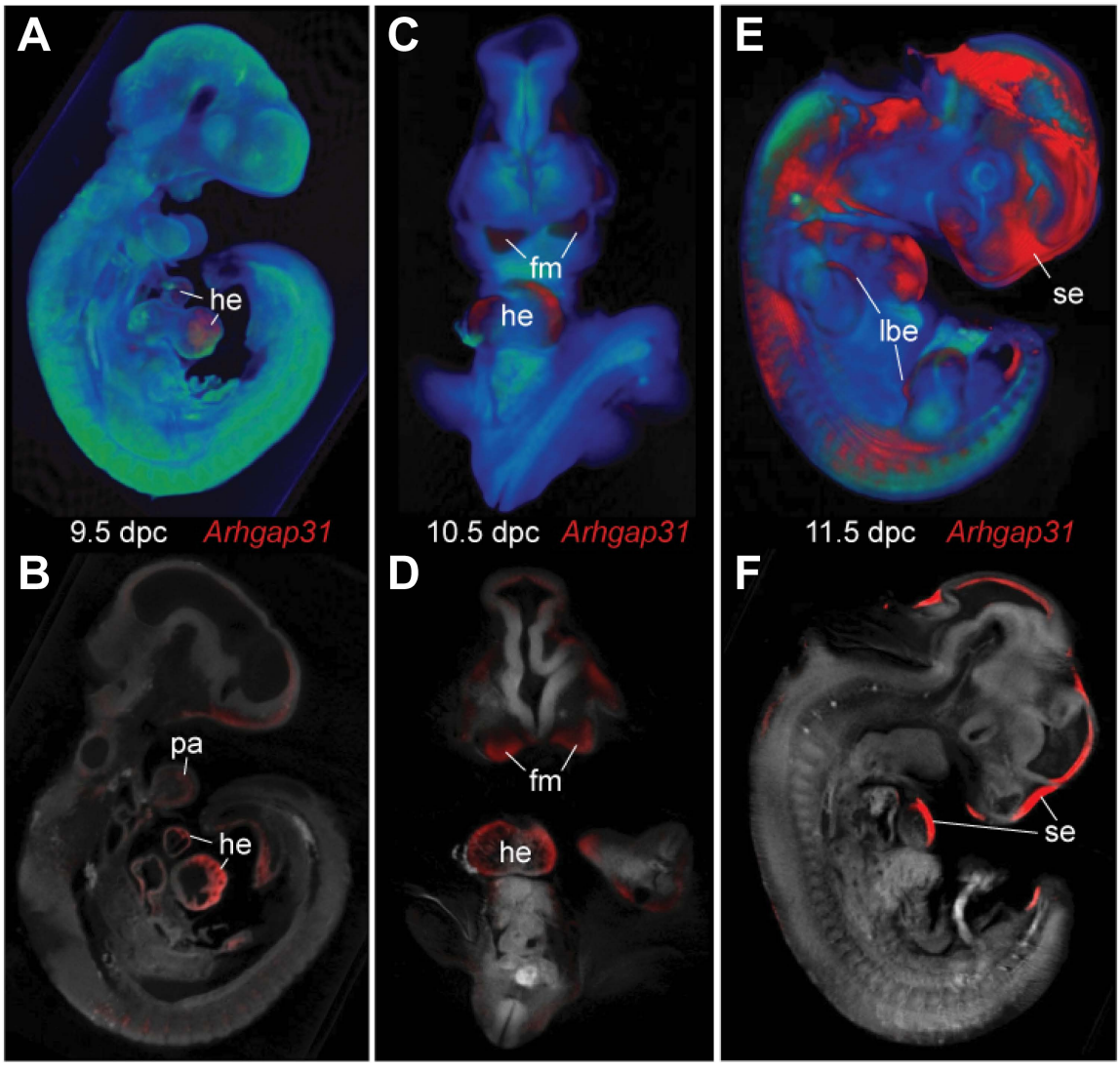
A
he
9.5 dpc Arhgap31
C
fm
he
10.5 dpc Arhgap31
E
se
lbe
11.5 dpc Arhgap31
B
pa
he
D
fm
he
F
se

Figure 3

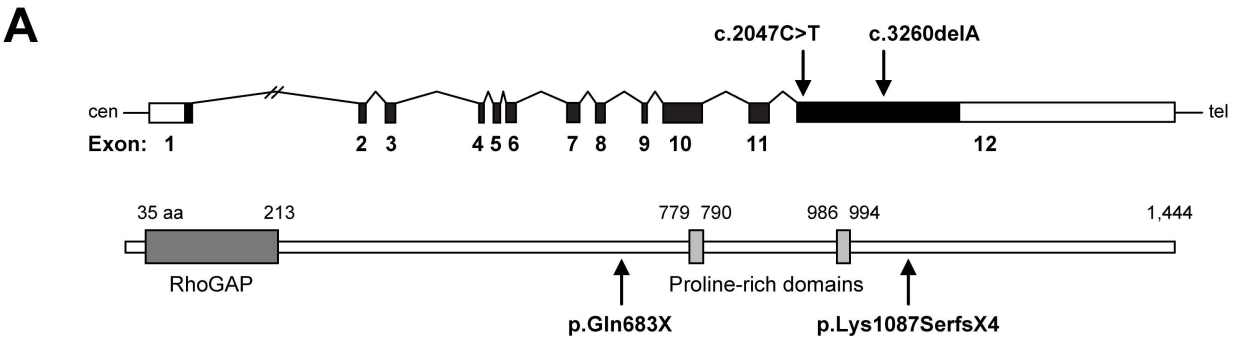
A
c.2047C>T
c.3260delA
cen
tel
Exon: 1 2 3 4 5 6 7 8 9 10 11 12
35 aa
213
779 790
986 994
1,444
RhoGAP
Proline-rich domains
p.Gln683X
p.Lys1087SerfsX4

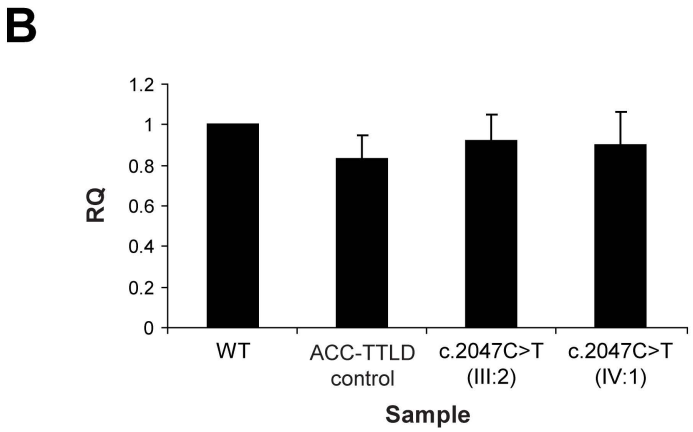
B
RQ
1.2
1
0.8
0.6
0.4
0.2
0
WT
ACC-TTLD control
c.2047C>T (III:2)
c.2047C>T (IV:1)
Sample

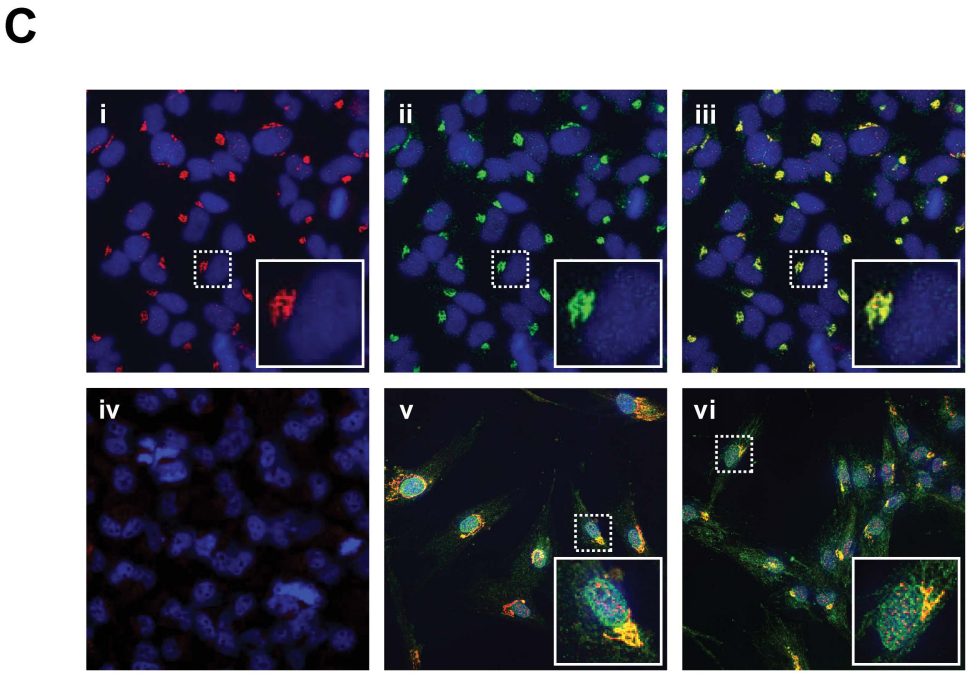
C
i
ii
iii
iv
v
vi

Figure 4

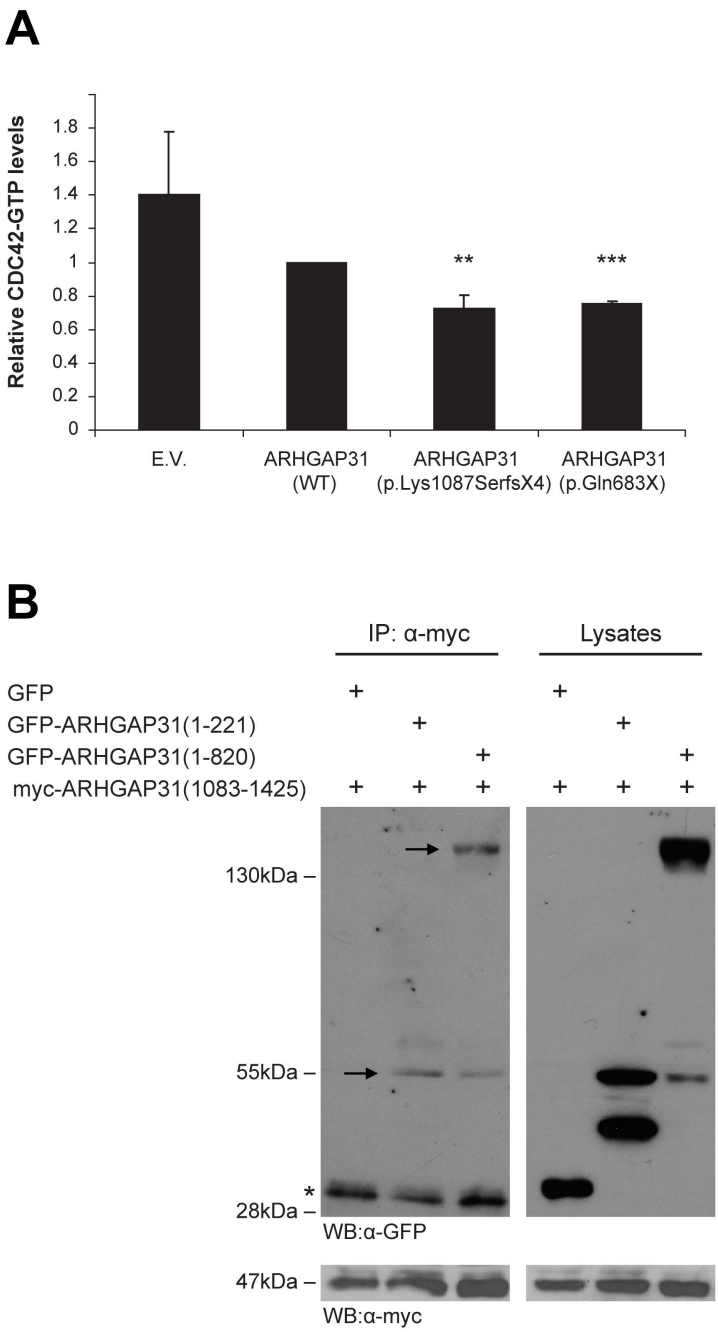
A
Relative CDC42-GTP levels
1.8
1.6
1.4
1.2
1
0.8
0.6
0.4
0.2
0
**
***
E.V.
ARHGAP31 (WT)
ARHGAP31 (p.Lys1087SerfsX4)
ARHGAP31 (p.Gln683X)
B
IP: α-myc
Lysates
GFP
GFP-ARHGAP31(1-221)
GFP-ARHGAP31(1-820)
myc-ARHGAP31(1083-1425)
130kDa –
55kDa –
28kDa –
*
WB:α-GFP
47kDa –
WB:α-myc

Figure 5

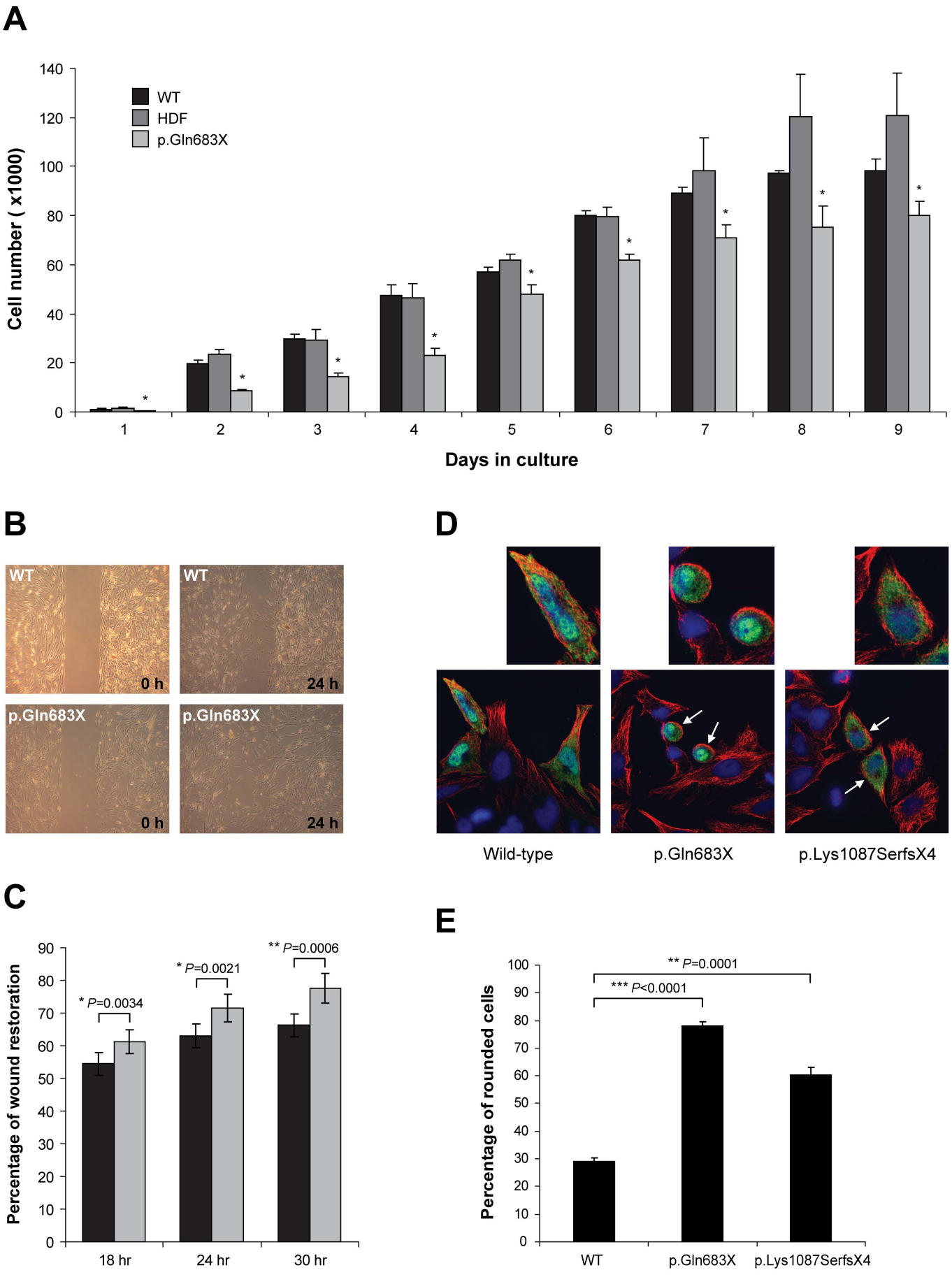
A
WT
HDF
p.Gln683X
Cell number (x1000)
Days in culture
B
WT
0 h
WT
24 h
p.Gln683X
0 h
p.Gln683X
24 h
C
Percentage of wound restoration
* P=0.0034
* P=0.0021
** P=0.0006
18 hr
24 hr
30 hr
D
Wild-type
p.Gln683X
p.Lys1087SerfsX4
E
Percentage of rounded cells
** P=0.0001
*** P<0.0001
WT
p.Gln683X
p.Lys1087SerfsX4

Figure 6

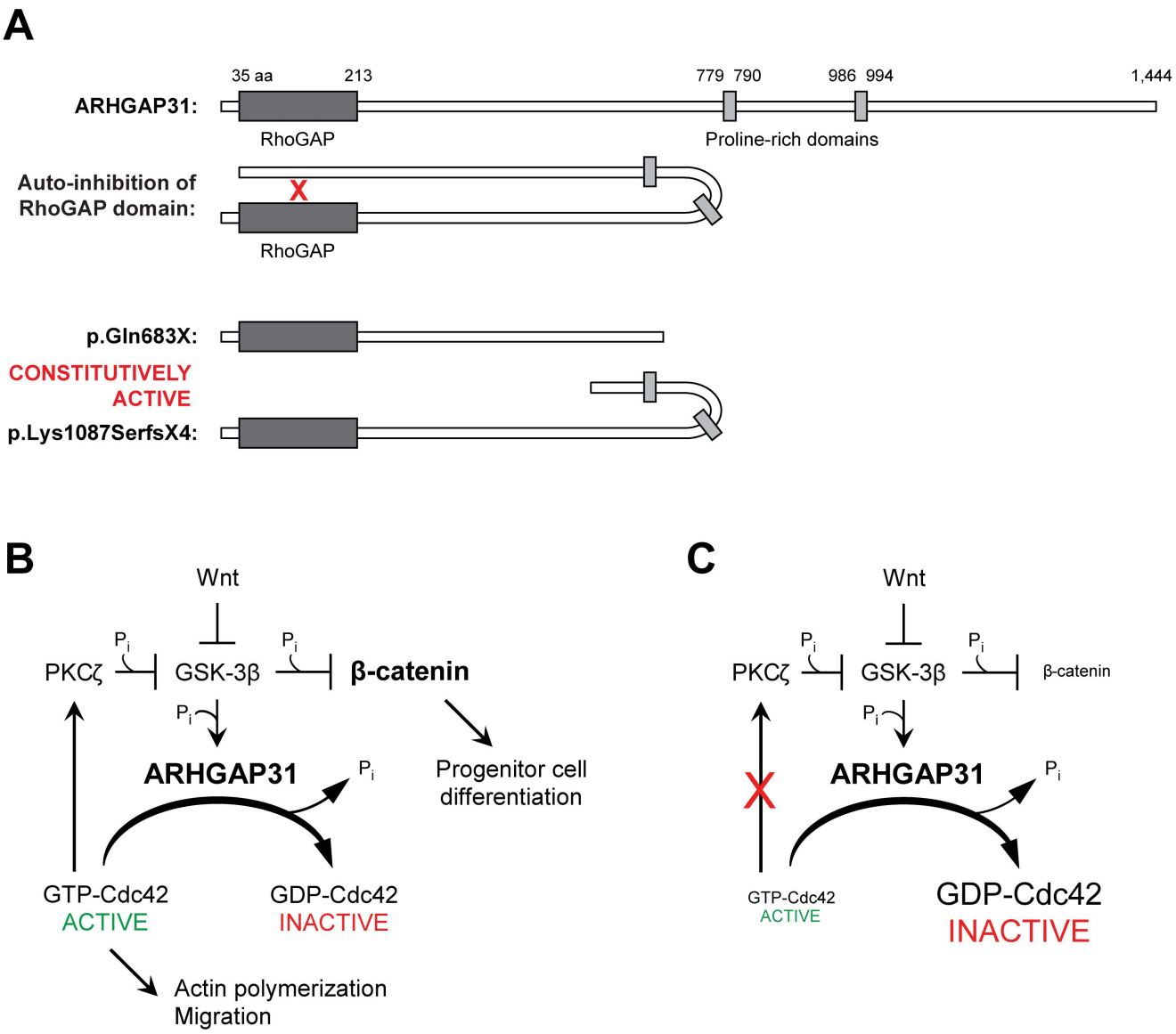
A
35 aa
213
779 790
986 994
1,444
ARHGAP31:
RhoGAP
Proline-rich domains
Auto-inhibition of RhoGAP domain:
X
RhoGAP
p.Gln683X:
CONSTITUTIVELY ACTIVE
p.Lys1087SerfsX4:
B
Wnt
Pi
PKCζ
GSK-3β
β-catenin
ARHGAP31
Progenitor cell differentiation
GTP-Cdc42
ACTIVE
GDP-Cdc42
INACTIVE
Actin polymerization
Migration
C
Wnt
PKCζ
GSK-3β
β-catenin
X
ARHGAP31
GTP-Cdc42
ACTIVE
GDP-Cdc42
INACTIVE

SUPPLEMENTAL DATA

Gain-of-Function Mutations of *ARHGAP31*, a Cdc42/Rac1 GTPase Regulator, Cause Syndromic Cutis Aplasia and Limb Anomalies

Laura Southgate*, Rajiv D. Machado*, Katie M. Snape*, Martin Primeau, Dimitra Dafou, Deborah M. Ruddy, Peter A. Branney, Malcolm Fisher, Grace J. Lee, Michael A. Simpson, Yi He, Teisha Y. Bradshaw, Bettina Blaumeiser, William S. Winship, Willie Reardon, Eamonn R. Maher, David R. FitzPatrick, Wim Wuyts, Martin Zenker, Nathalie Lamarche-Vane & Richard C. Trembath
* these authors contributed equally to this work

CONTENTS:

Supplemental Figures:

Supplemental Figure 1: Complete results of the genome-wide linkage scan

Chromosome 1

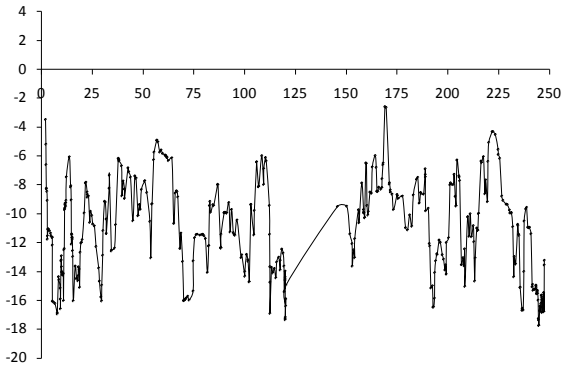

Chromosome 2

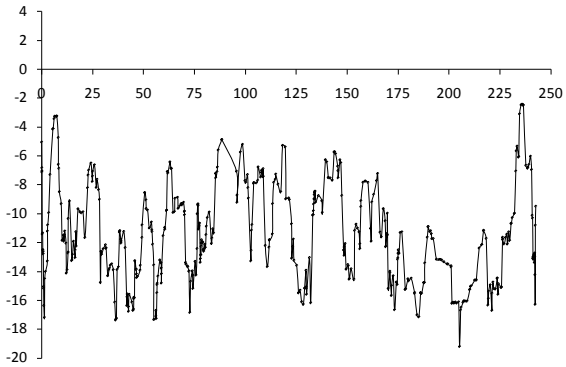

Chromosome 3

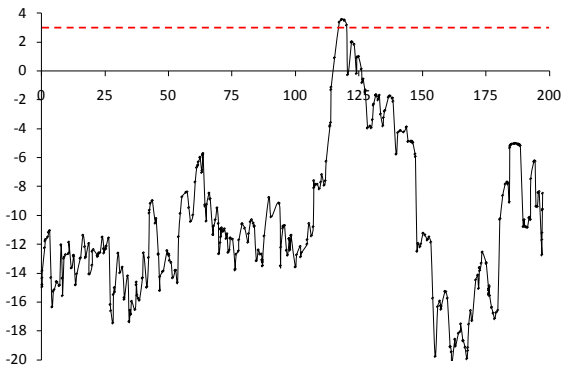

Chromosome 4

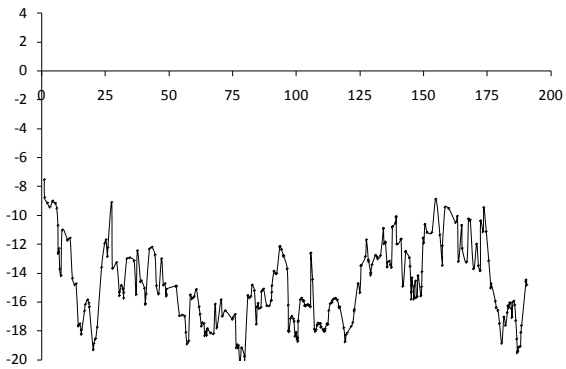

Chromosome 5

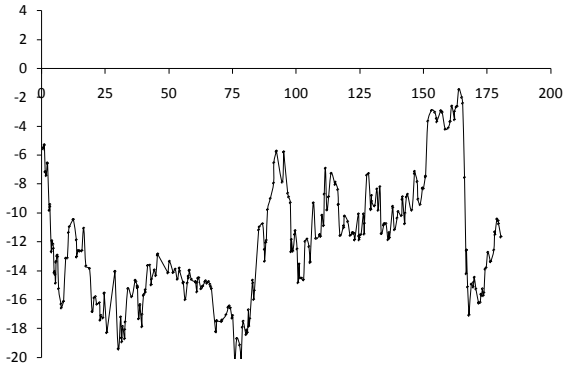

Chromosome 6

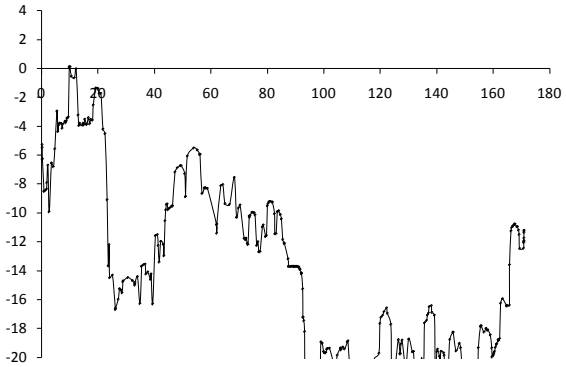

Supplemental Figure 1 (cont...)

Chromosome 7

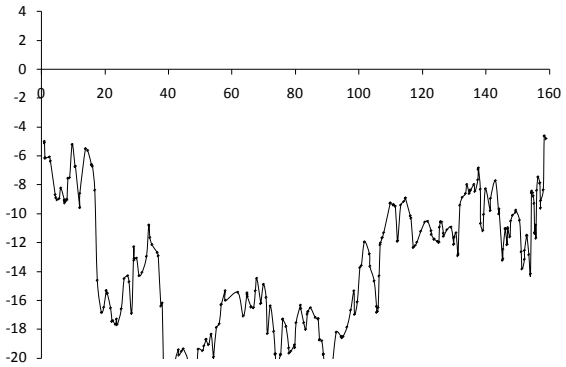

Chromosome 8

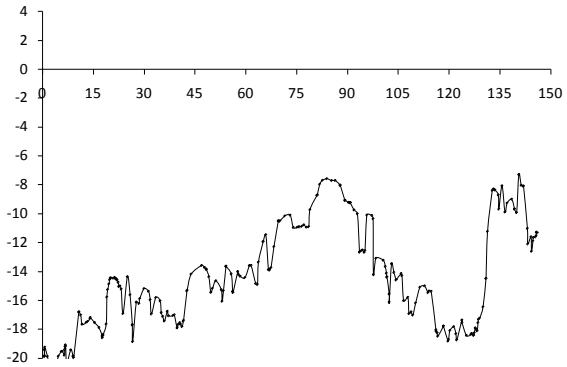

Chromosome 9

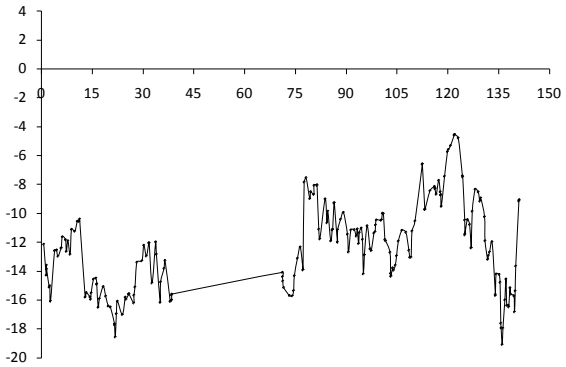

Chromosome 10

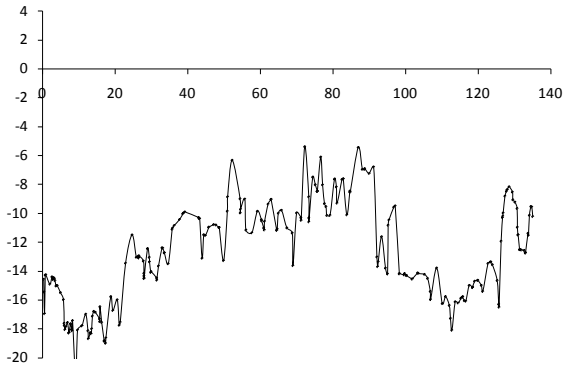

Chromosome 11

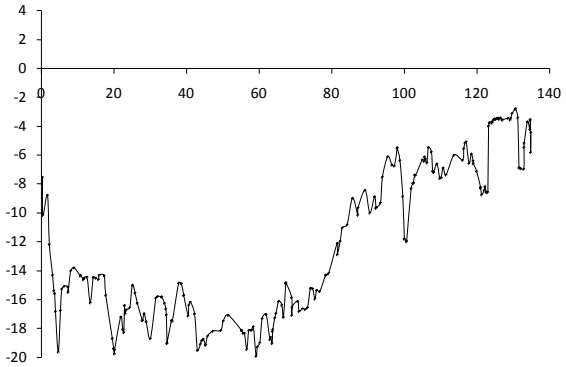

Chromosome 12

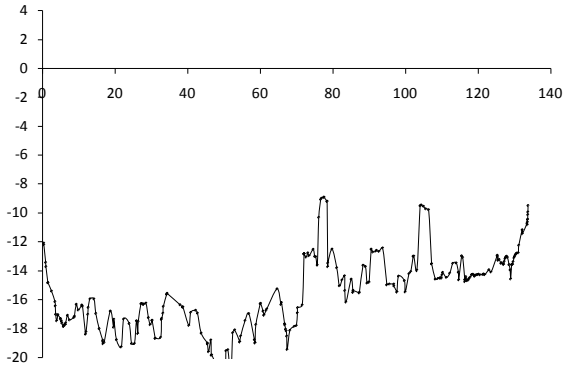

Supplemental Figure 1 (cont...)

Chromosome 13

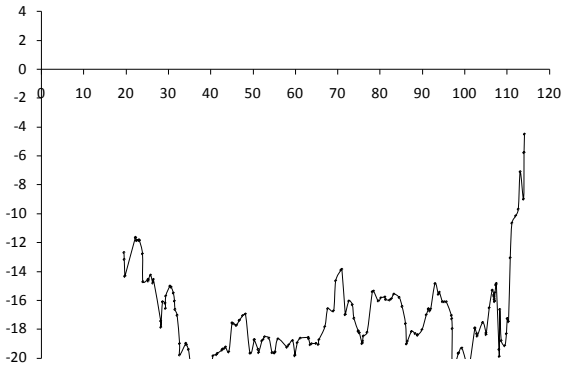

Chromosome 14

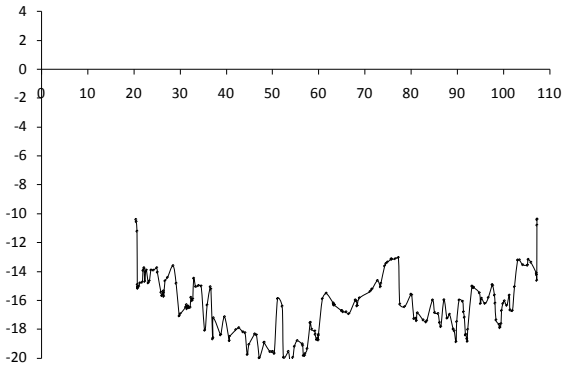

Chromosome 15

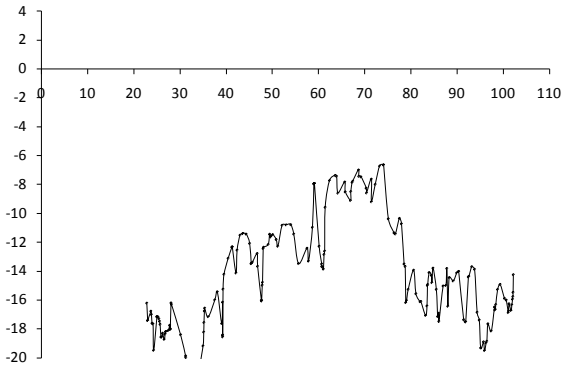

Chromosome 16

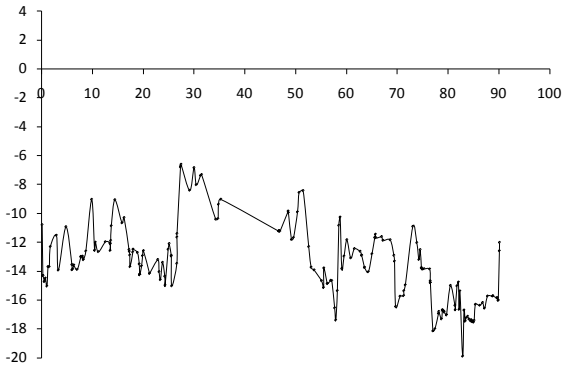

Chromosome 17

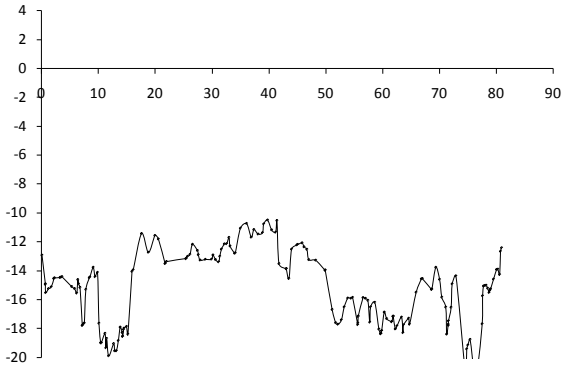

Chromosome 18

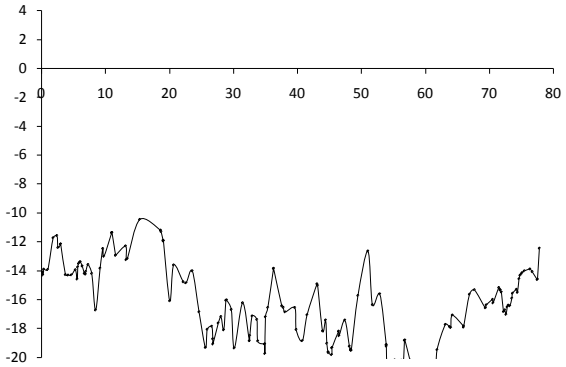

Supplemental Figure 1 (cont...)

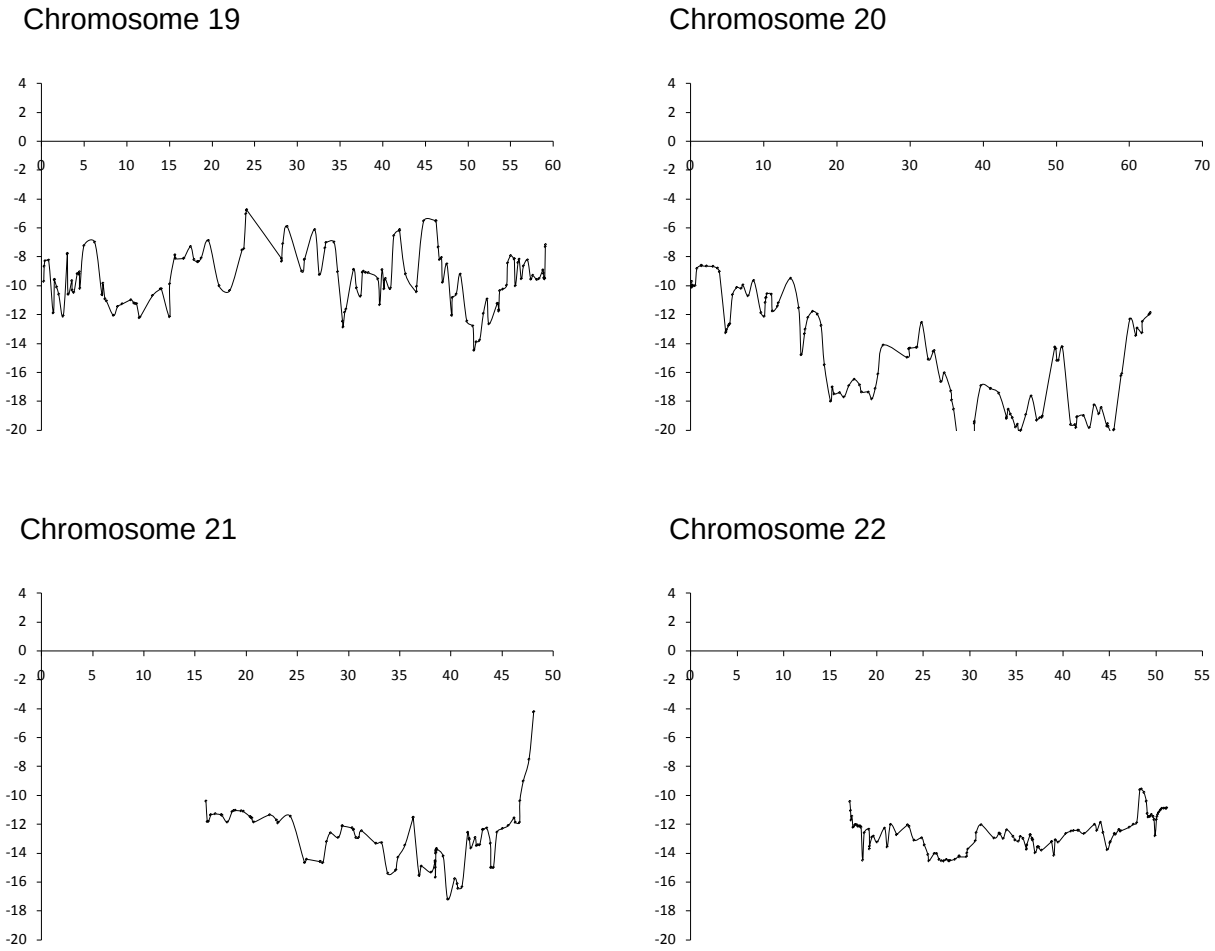

Graphs representing the combined linkage results for families AOS-5 and AOS-12 across all 22 autosomes. Chromosome numbers are written above each respective graph. Chromosomal positions in Mb, according to the hg19 genome build, are indicated on the x-axis. The y-axis denotes the LOD scores, as calculated using Merlin software using genotypes from a total of 5,657 SNPs. The linkage peak on chromosome 3q13, containing the *ARHGAP31* gene, is the only region that achieves a LOD score of genome-wide significance (i.e. LOD ≥ 3), as depicted by the dashed horizontal line in red.

Supplemental Figure 2: Refinement mapping and positional cloning of the ACC-TTLD phenotype

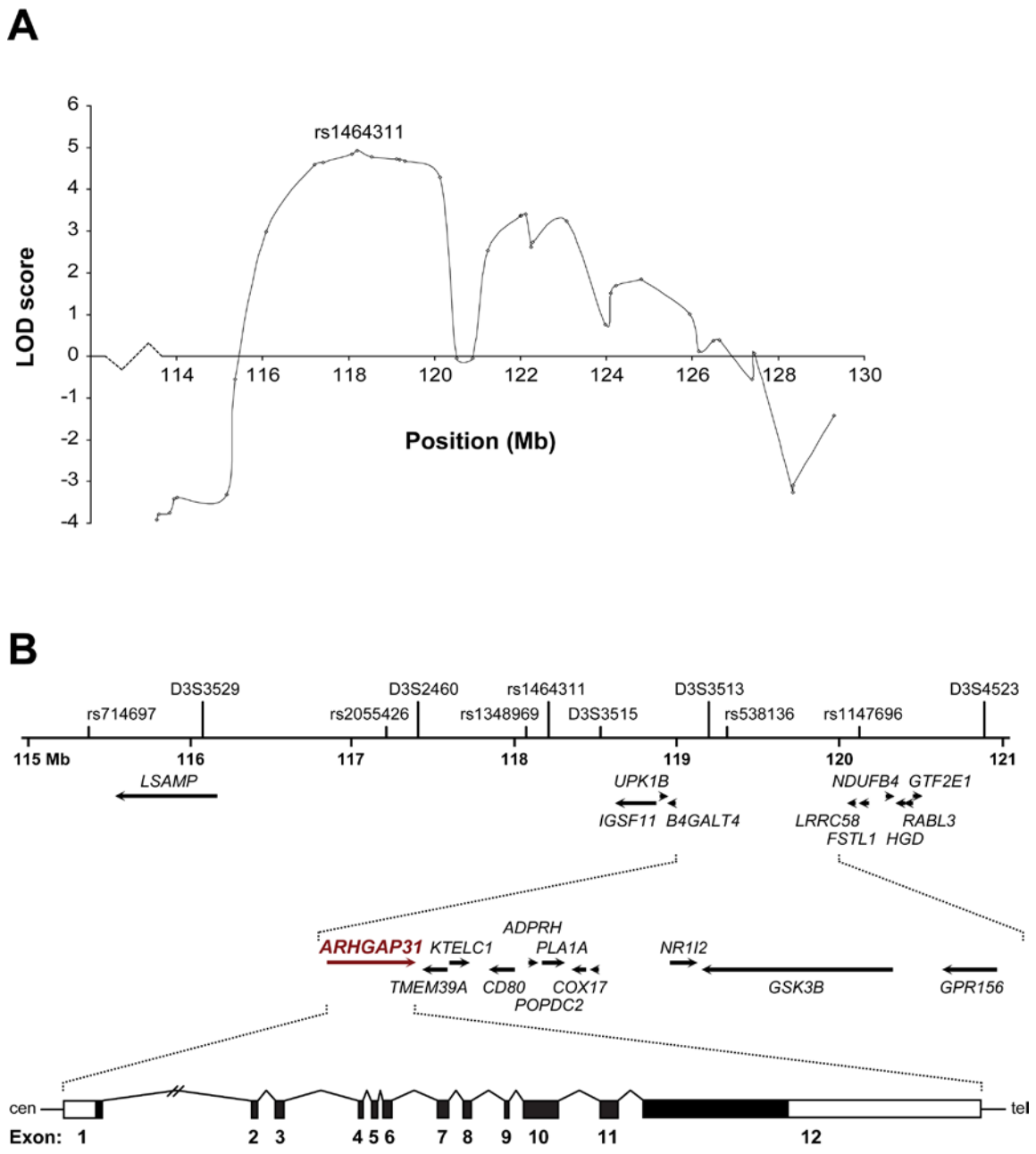

(A) Segment of chromosome 3, showing linkage results for families AOS-5 and AOS-12 to refine the critical interval. Using genotypes from a total of 36 SNPs and 8 microsatellites across 110–130 Mb, a maximum multipoint LOD score of 4.93 was achieved at marker rs1464311. The extended 13.2 Mb linkage interval examined by exome sequencing is defined by the accepted genome-wide criteria for exclusion (i.e. LOD ≤ -2).
(B) Physical map of the 5.53 Mb critical linkage interval on chromosome 3q13.31-q13.33 (flanked by markers rs714697 and D3S4523), showing the 21 genes within the region and the relative location of *ARHGAP31*. The *ARHGAP31* gene structure is expanded beneath.

Supplemental Figure 3: *ARHGAP31* transcript expression

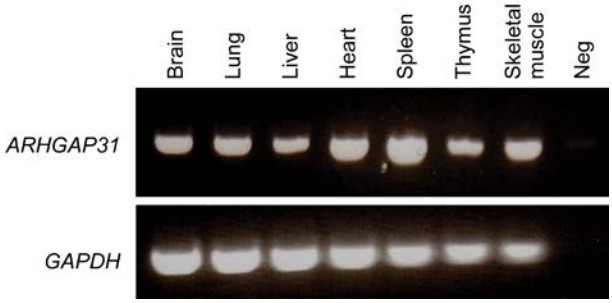

PCR amplification of *ARHGAP31* in a human fetal cDNA tissue panel demonstrates global expression of the gene. *GAPDH* primers were used to amplify a 983 bp fragment from all tissues as an internal control. Neg = no DNA control.

Supplemental Figure 4: Western blot quantification for G-LISA assays

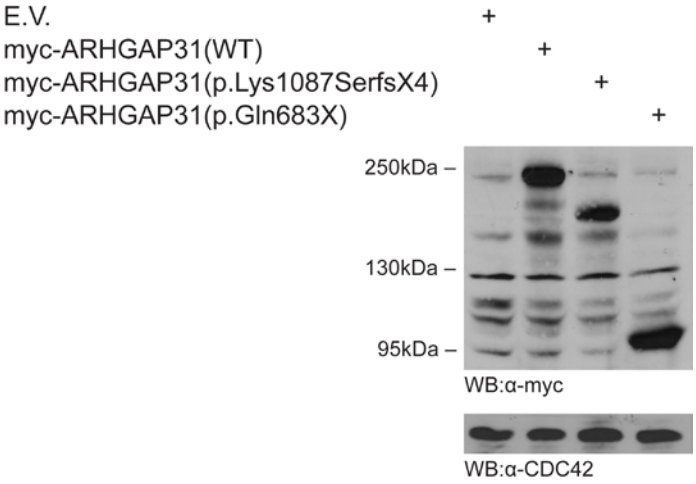

Western blot to determine the levels of tagged proteins and Cdc42 for used in G-LISA assays. A myc-specific antibody was used to detect WT and mutant (p.Lys1087SerfsX4 and p.Gln683X) proteins. E.V. = empty vector.